



Electrodeposition of bismuth telluride thermoelectric films from a nonaqueous electrolyte using ethylene glycol

Hai P. Nguyen^a, Minxian Wu^a, Jiale Su^b, Ruud J.M. Vullers^b, Philippe M. Vereecken^{c,d}, Jan Fransaer^{a,*}

^a Department of Metallurgy and Materials Engineering, KU Leuven, Heverlee, Belgium

^b imec/Holst Centre, Eindhoven, The Netherlands

^c imec, Heverlee, Belgium

^d Center for Surface Chemistry and Catalysis, KU Leuven, Heverlee, Belgium

ARTICLE INFO

Article history:

Received 23 November 2011

Received in revised form 25 January 2012

Accepted 25 January 2012

Available online 23 February 2012

Keywords:

Thermoelectric
Bismuth telluride
Electrodeposition
High rate
Ethylene glycol

ABSTRACT

Ethylene glycol was studied as an electrolyte for the electrodeposition of thermoelectric bismuth telluride films by cyclic voltammetry, rotating ring disk electrode and electrochemical quartz crystal microbalance (EQCM). The reduction of both Bi^{3+} and Te^{4+} ions proceeds in one step without the formation of intermediates at potentials more negative than +0.2 V and +0.55 V vs. SHE, respectively. The diffusion coefficients and the rate constants for reduction were found to be similar for Bi and Te. Stoichiometric Bi_2Te_3 films with a uniform composition profile were obtained from solutions containing up to 1 M of $\text{Bi}(\text{NO}_3)_3$ and TeCl_4 , at current densities up to 5 A dm^{-2} ($\sim 102 \mu\text{m h}^{-1}$). Both p- and n-type bismuth telluride films could be obtained, as confirmed by Seebeck coefficient measurements.

© 2012 Elsevier Ltd. All rights reserved.

1. Introduction

Bismuth telluride and its derivatives doped with antimony and selenium are the best-known materials for room temperature thermoelectric applications [1,2]. Electrodeposition has been recognized as an effective method for preparing these materials due to its unique features: simple, fast, low-cost, and capable of selective deposition. The number of publications on electrodeposition of thermoelectric materials, particularly bismuth telluride based materials, has increased by a factor of three in the last decade [3]. Most of these studies dealt with the electrodeposition of bismuth telluride from acidic solutions using 1 M HNO_3 that can dissolve only about 20 mM Te species, which in turn limits the Bi concentration in order to obtain the correct alloy composition (Bi_2Te_3) [4–9]. The low metal ion concentration causes composition inhomogeneities across the film thickness due to the unbalanced depletion of Bi and Te species in plating bath. The rather low mass transport in solution also limits the maximum deposition current and hence growth rate that can be attained. The highest reported deposition current density is 1.6 A dm^{-2} which corresponds to about $34 \mu\text{m h}^{-1}$ [8]. In addition, it was reported that it was difficult to obtain p-type Bi_2Te_3 films from nitric acid bath [5]. So

far, Glatz et al. were the only researchers that reported the electrodeposition of thick p-type Bi_2Te_3 films at a rate of $50 \mu\text{m h}^{-1}$ [9]. However, 2 M nitric acid was required to maintain higher solubility of Te (80 mM) and a complex pulsed deposition method was utilized.

Non-aqueous electrolytes often provide advantages such as wide electrochemical window, good thermal stability, high metal ion solubility. Tellurium and tellurium alloys films have been electrochemically prepared from dimethyl sulfoxide (DMSO) [10,11] and dimethyl formamide (DMF) [12]. Bismuth antimony thermoelectric nanowires was prepared from DMSO [13]. Li and coworkers have used DMSO for the electrodeposition of bismuth telluride and bismuth antimony telluride materials [14,15]. In our previous work [16], we have examined the effects of various parameters such as bath composition, total metal concentration, and temperature on the composition and morphology of Bi_2Te_3 films deposited from DMSO electrolytes. We found that film composition was very sensitive to temperature as almost pure Te films were obtained if the temperature rose slightly above room temperature, which somewhat limits the use of DMSO-base electrolytes for Bi_2Te_3 .

In this work, the use of ethylene glycol (EG) is investigated as an electrolyte for Bi_2Te_3 deposition. Ethylene glycol (EG) is an organic solvent with a relatively high dielectric constant ($\epsilon = 37.7$). It is known to dissolve various metal salts that are only sparingly soluble in water and was used for the electrodeposition of compounds that are difficult to deposit from aqueous electrolytes such as CdSe

* Corresponding author. Tel.: +32 16321239; fax: +32 16321991.

E-mail address: jan.fransaer@mtm.kuleuven.be (J. Fransaer).

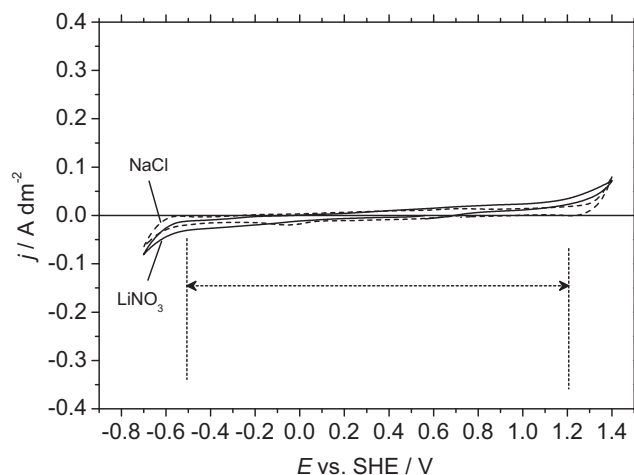


Fig. 1. Current vs. potential curves obtained from EG solutions containing either 0.5 M LiNO₃ or 0.5 M NaCl, at 50 °C, scan rate 20 mV s⁻¹, Pt WE (ϕ 4 mm). Similar electrochemical windows of 1.7 V are indicated for both solutions.

[17], ZnSb [18], and AuSn [19]. Due to its high boiling temperature (197 °C) and low vapor pressure (8 Pa at room temperature), EG allows electrodeposition at high temperature, which was reported to improve crystallization of CdS_xSe_{1-x} films for solar cell applications [20]. In this work, we used ethylene glycol as a solvent for electrodeposition of bismuth telluride films for thermoelectric applications. We studied the deposition mechanism of Bi, Te, and Bi_xTe_y, the effects of various parameters on the deposits, and very high rate deposition of stoichiometric bismuth telluride films from concentrated electrolytes.

2. Experimental

Bismuth nitrate pentahydrate (Bi(NO₃)₃·5H₂O, Alfa Aesar, >98%) and tellurium tetrachloride (TeCl₄, Alfa Aesar, 99%) were used as sources of metal ions. Lithium nitrate (LiNO₃, Sigma-Aldrich, 99%) was added up to 0.5 M to improve electrolyte conductivity. Electrolytes were prepared by dissolving the salts in EG (Alfa Aesar, 99%) without further treatment. The solutions were then stirred at room temperature until completely transparent. Concentrations of bismuth and tellurium were fixed at 0.05 M each, unless mentioned otherwise. All the experiments were carried out with a three electrode setup in ambient environment at 50 °C except for some experiments where the influence of temperature was investigated. The reference electrode was a Pt wire immersed in an ethylene glycol solution containing 0.002 M of ferrocene/ferrocenium and 1 M LiNO₃ as a supporting electrolyte. However, potentials reported in this work were converted to the standard hydrogen electrode (SHE) using the potential of our reference electrode, +0.5 V vs. the SHE. The counter electrode was a Pt mesh. Different working electrodes (WE) were used in different experiments as mentioned below.

An electrochemical quartz crystal microbalance (EQCM, Maxtek) and a potentiostat (EG&G 273) were connected to simultaneously monitor potential, current and resonant frequency change of the quartz crystal (5 MHz Ti/Pt AT cut, ϕ 1.27 cm, Maxtek, CA). The mass change of the quartz crystals was calculated based on the Sauerbrey equation:

$$\Delta f = C_f \Delta m \quad (1)$$

where Δf (Hz) is the change in the resonance frequency of the crystal due to the change in mass Δm ($\mu\text{g cm}^{-2}$) of the crystal; C_f (Hz $\mu\text{g}^{-1} \text{cm}^2$) is a conversion coefficient. Because the coefficient C_f is strongly affected by parameters such as viscosity of the

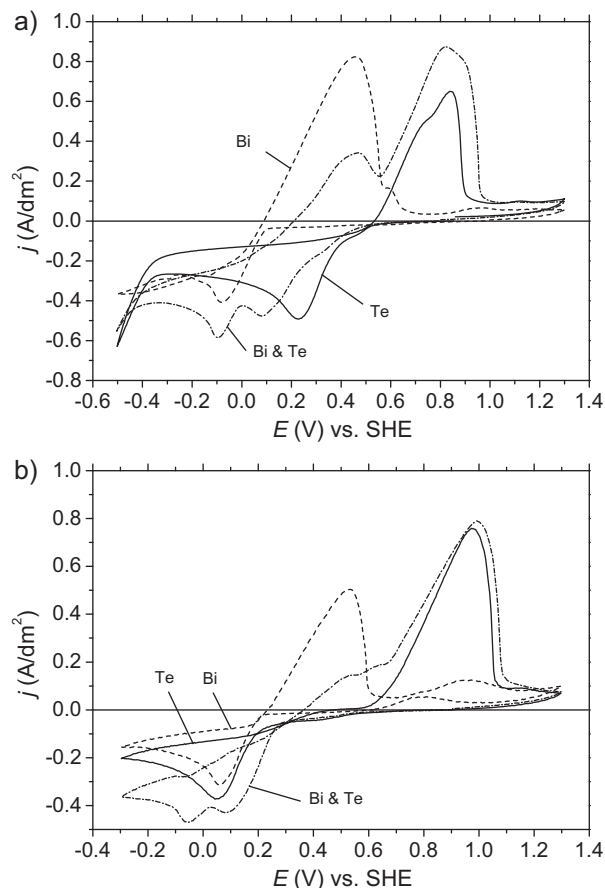


Fig. 2. Cyclic voltammograms obtained from EG solutions containing different conducting salts: 0.5 M LiNO₃ (a) or 0.5 M NaCl (b) and either 0.05 M Bi(NO₃)₃ (dashed line) or 0.05 M TeCl₄ (solid line) or both (dash-dotted line), at 50 °C, scan rate 20 mV s⁻¹, WE Pt ϕ 4 mm. Reductions of Bi and Te are largely different in the solutions containing TeCl₄.

electrolyte and surface morphology of the deposits [21], we calibrated our EQCM electrodes based on the electrodeposition and stripping of Bi films at several potentials from an EG solution containing 50 mM Bi(NO₃)₃ and 0.5 M LiNO₃ and the C_f was determined to be 40.2 Hz $\mu\text{g}^{-1} \text{cm}^2$.

A rotating ring disk electrode (RRDE) (Ametek, model RDE0071, $\phi_{\text{disk}} = 4.57$ mm, $\phi_{\text{innerring}} = 4.93$ mm, $\phi_{\text{outerring}} = 5.38$ mm, collection

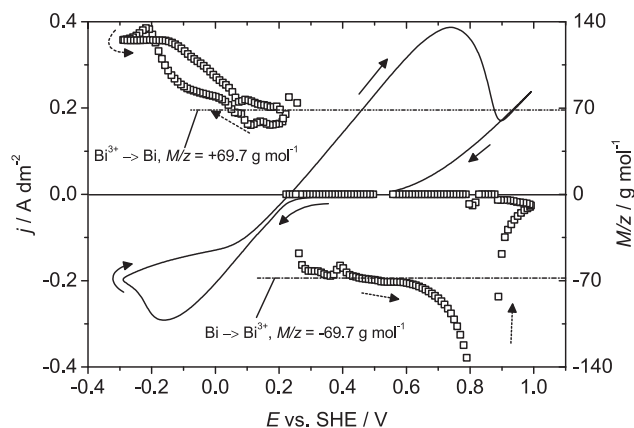


Fig. 3. Cyclic voltammogram and M/z values obtained for a Bi solution containing 0.05 M Bi(NO₃)₃ and 0.5 M LiNO₃, at 50 °C, scan rate 20 mV s⁻¹, Pt WE (EQCM crystal).

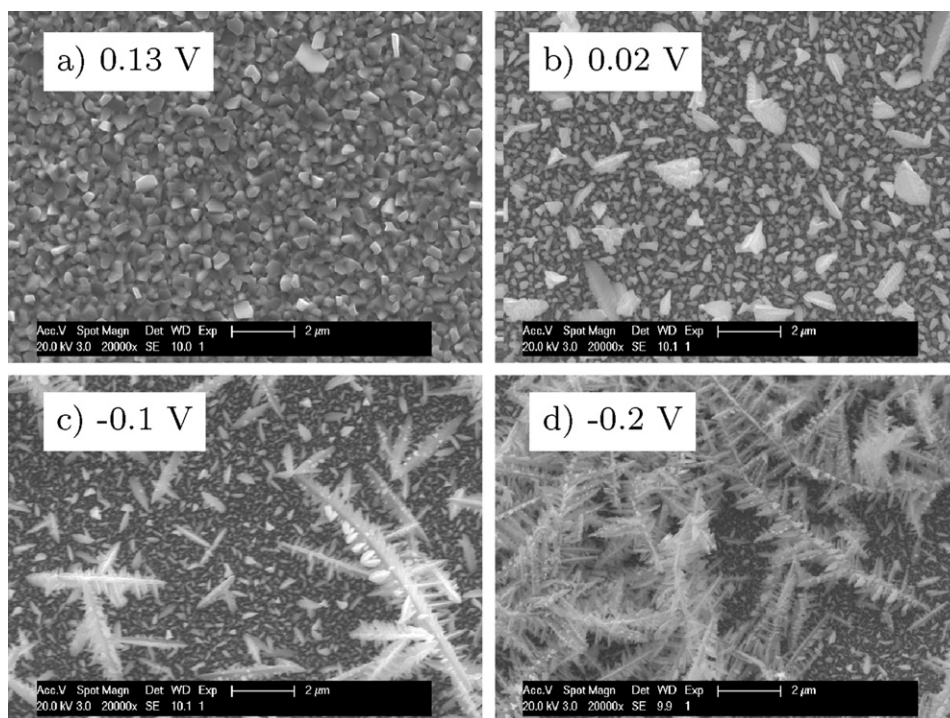


Fig. 4. SEM images of Bi films deposited at different potentials from a Bi solution containing 0.05 M $\text{Bi}(\text{NO}_3)_3$ and 0.5 M LiNO_3 , 50 °C, non-stirred (scale bar 2 μm).

efficiency 22%) was used to examine the existence of soluble reduction products in the Te solution. Polarization curves from individual Bi and Te solutions were measured at different rotation speeds using a platinum rotating disk electrode ($\phi 4$ mm). The Koutecky–Levich equation was applied following the method introduced in [22] to determine diffusion coefficients of bismuth and tellurium and rate constants of their reductions.

Bismuth telluride films were prepared in potentiostatic mode on Au-coated silicon wafers. The morphology of the deposited films were analyzed by a scanning electron microscope (SEM, Philip XL30). The atomic ratios of Bi and Te in the deposited films were analyzed by energy-dispersive X-ray (EDX).

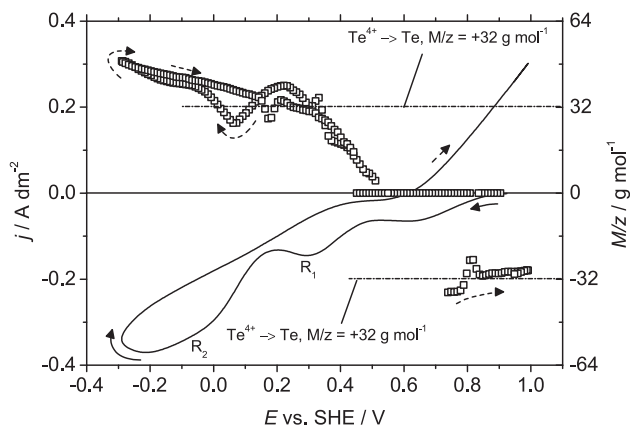


Fig. 5. Cyclic voltammogram and M/z values obtained for a Te solution containing 0.05 M TeCl_4 and 0.5 M LiNO_3 , at 50 °C, scan rate 20 mV s^{-1} , Pt WE (EQCM crystal).

3. Results and discussion

3.1. Electrochemical behaviors

In order to enhance the ionic conductivity of the EG, either 0.5 M NaCl or 0.5 M LiNO_3 was used as supporting electrolytes. As can be seen from Fig. 1, both solutions have the same electrochemical window of 1.7 V (from -0.5 V to 1.2 V vs. SHE), which is a bit larger than the electrochemical window of water (1.24 V). However, the supporting electrolytes were found to have a marked influence on the reduction potential of bismuth and tellurium. Fig. 2a shows cyclic voltammograms (CV) of Bi, Te, and mixed solutions in presence of 0.5 M NaCl . Reduction peak for bismuth and tellurium are situated at -0.08 V and $+0.22$ V, respectively. When LiNO_3 is used as supporting electrolyte, both reduction peaks almost coincide as shown in Fig. 2b, which is very advantageous for the electrodeposition of alloys. For this reason, LiNO_3 was used in all further experiments.

Cyclic voltammograms and EQCM data from the individual Bi, Te solutions were analyzed for M/z based on Faraday's law:

$$\frac{M}{z} = F \frac{\Delta m}{j \Delta t} \quad (2)$$

where M (g mol^{-1}) is the molar mass of the reducing/oxidizing agent; z is the number of electrons involved in the electrochemical reaction; $F = 96,500$ (C mol^{-1}) is the Faraday constant; Δm (g cm^{-2}) is the mass change of the working electrode caused by current density j (A cm^{-2}) passing in a time span Δt (s). Because the theoretical value of this ratio can be calculated for any electrochemical reaction, electrochemical processes can be examined by comparing the experimental to the theoretical M/z value. Furthermore, the M/z ratio given by Eq. (2) can also be estimated as a function of applied potential, which allows to examine changes in reaction mechanisms along a CV. However, when the current in CV goes through zero, experimentally determined M/z values become uncertain. Therefore, any conclusion drawn in these zones should

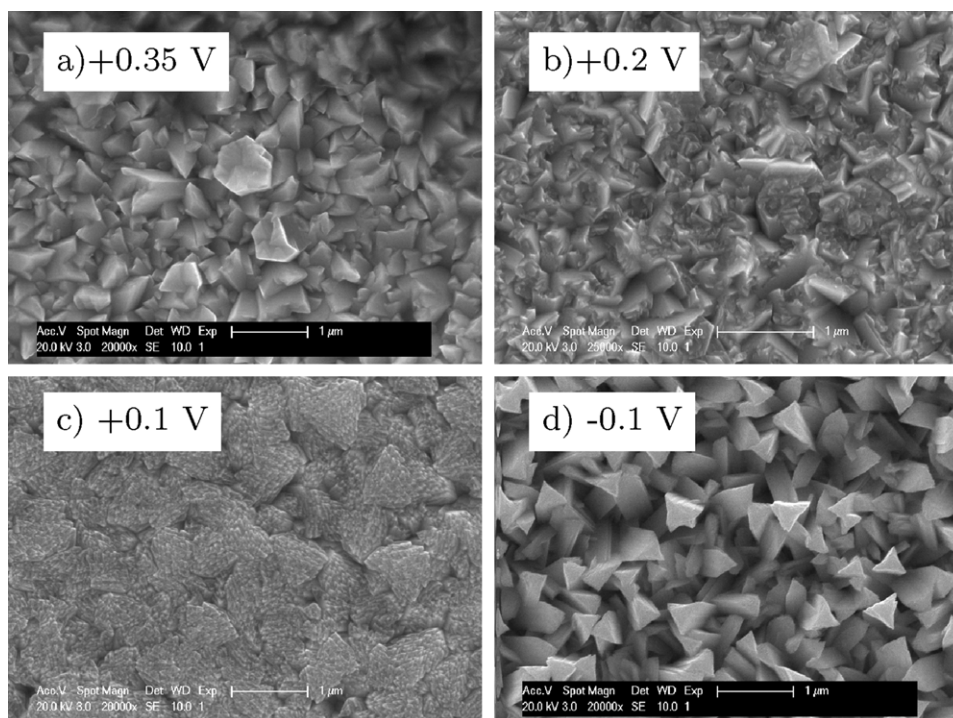
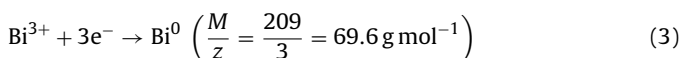


Fig. 6. SEM images of Te films deposited at different potentials from a Te solution containing 0.05 M TeCl_4 and 0.5 M LiNO_3 at 50 °C, non-stirred (scale bar 1 μm).

be avoided [23]. In this paper, we use the magnitude of current density $|j|$ in Eq. (2), so that M/z has the same sign as Δm , i.e. positive for deposition and negative for a dissolution process.

Fig. 3 shows the CV and EQCM data obtained from a solution containing 0.05 M $\text{Bi}(\text{NO}_3)_3$ and 0.5 M LiNO_3 . The reduction starts around +0.2 V and between +0.2 V and 0.07 V, the M/z value is constant and roughly equal to +69 g mol^{-1} which corresponds to the theoretical value for the three-electron reduction of Bi^{3+} to Bi^0 :



The reduction potential of Bi in the EG electrolyte is similar to the value +0.2 V obtained in aqueous solution at a pH between -2.0 and +2.0 [24]. Bismuth films deposited in this potential region are smooth and compact as shown by SEM images in Fig. 4a and b.

At more negative potentials (+0.07 to -0.3 V), M/z increases up to 130 g mol^{-1} . It was observed that the films start to growing dendritically at these more negative potentials, as can be seen in Fig. 4, which alters the sensitivity of the quartz crystal according to Vatankeh et al. [21]. Hence, the higher M/z values are not a result of a change in the three-electron reduction mechanism, but are due to a decrease of the sensitivity of the QCM crystal. This was also confirmed by the increase in the damping of the crystal that was noticed in this potential range.

During the anodic scan, oxidation starts at +0.23 V with M/z of about -69.7 g mol^{-1} , which corresponds to the dissolution of Bi to Bi^{3+} . The dissolution continues up to +0.77 V where the oxidation current shows a maximum and M/z increases strongly. The increase in M/z are observed at the end of the dissolution process, when some parts of Pt electrode become expose to the solution forming a galvanic couple with the remaining Bi. This leads to galvanic corrosion which leads to an overestimation of M/z . Hence, Bi also anodically dissolves in a one-step three-electron process.

As the Bi layer dissolves, the current decreases but then increases at potentials more positive than +0.9 V. On the backward scan, the current decreases to zero at +0.55 V vs. SHE. During this process, no mass change is detected on the EQCM and M/z remains

zero. Because this current is not observed when measuring on the small (bulk) Pt (see Fig. 1), it is believed to relate to the working electrode rather than decomposition of the solvent. In order to confirm this phenomenon, we carried out CVs from LiNO_3 0.5 M solution using a piece of Pt-coated Si wafer as working electrode and observed a similar current. Because both Pt/Si and Pt/quartz electrode have a thin Ti adhesion layer, the current may be caused by reactions of Ti or on Ti.

Fig. 5 shows the CV obtained for an EG solution containing 0.05 M TeCl_4 and 0.5 M LiNO_3 . The first wave (with zero M/z) starts from open circuit potential +0.9 V and ends at +0.55 V. This reduction current is also observed where a piece of Pt-coated silicon wafer is used as the working electrode. However, it does not appear if CVs are carried out on a small-bulk Pt electrode, as shown in Fig. 2b. We attribute this wave to artifacts of the thin film working

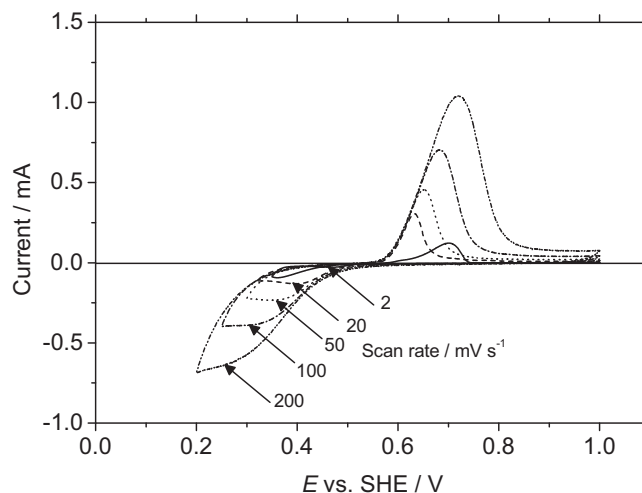


Fig. 7. Cyclic voltammograms obtained at different scan rates from 2 to 200 mV s^{-1} for a Te solution containing 0.05 M TeCl_4 and 0.5 M LiNO_3 , at 50 °C, Pt WE (RRDE).

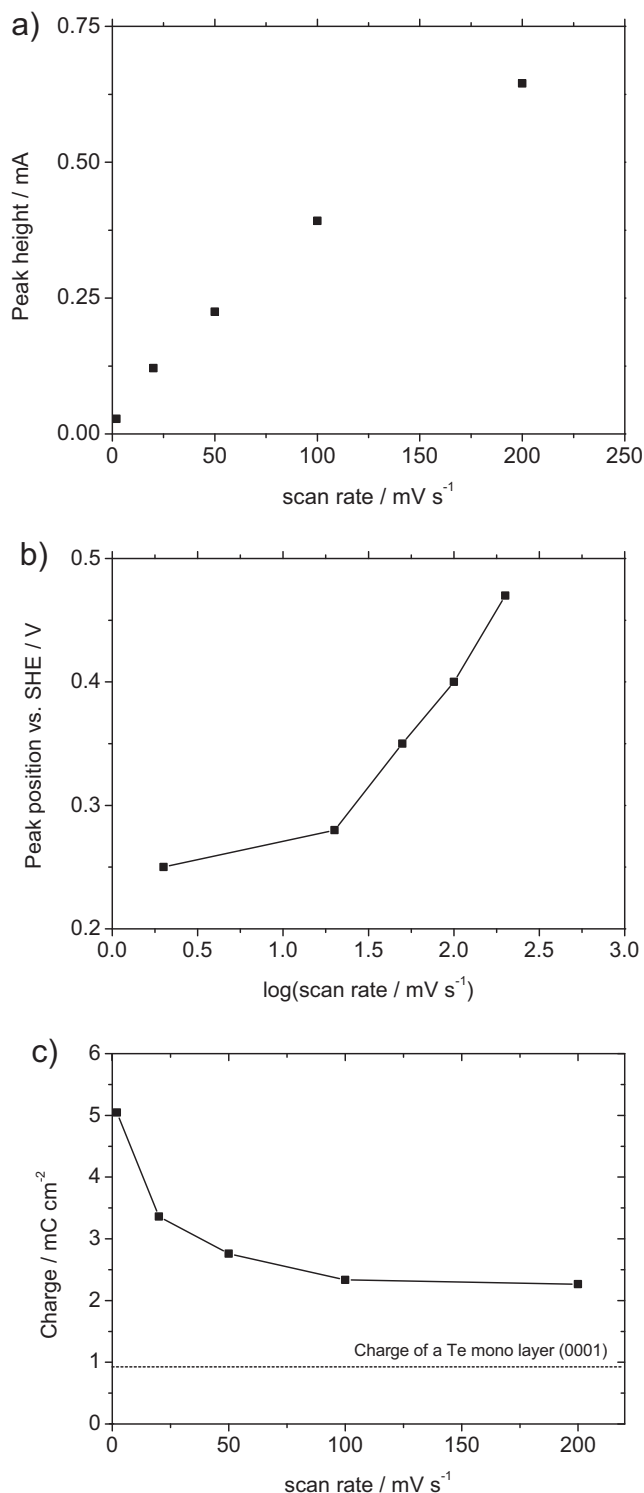


Fig. 8. Dependence of position (a), height (b) and charge (c) of the peak R_1 (in Fig. 5) with respect to scan rate from 2 to 200 mV s^{-1} for a solution contains 0.05 M TeCl_4 and 0.5 M LiNO_3 , at 50 °C, non-stirred, Pt WE (RRDE).

electrode, probably reactions of the Ti adhesion layer underneath the Pt layer on the quartz crystal or silicon wafer.

Bulk Te deposition can be observed at potentials more negative than +0.3 V (peak R_2) with M/z of approximately $+32 \text{ g mol}^{-1}$, corresponding to the four-electron reduction of Te^{4+} :

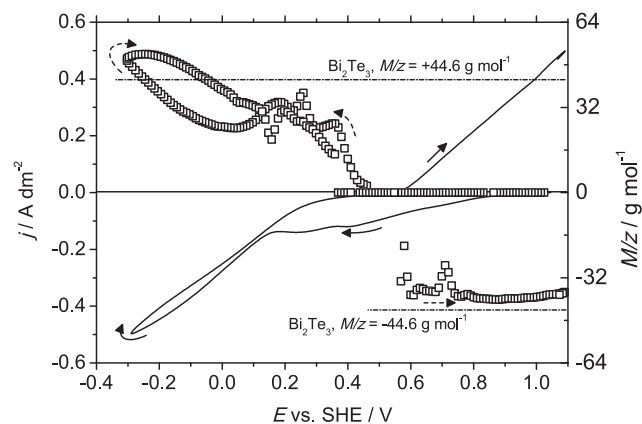


Fig. 9. Cyclic voltammogram and M/z values obtained for a mixed solution containing 0.05 M $\text{Bi}(\text{NO}_3)_3$, 0.05 M TeCl_4 , and 0.5 M LiNO_3 , at 50 °C, scan rate 20 mV s^{-1} , Pt WE (EQCM crystal).

The slightly increasing M/z ratio obtained at lower potentials can be explained by the roughening of the Te surface, as shown in Fig. 6c and d, and also indicated by the concomitant increase in the damping of the quartz crystal.

The M/z values corresponding to the reduction peak R_1 are between 0 and $+32 \text{ g mol}^{-1}$. This can occur if two electrochemical processes occur in parallel this potential range, one with an $M_1/z_1 = 0$ and one with an $M_2/z_2 = 32$, where the latter process corresponds to the 4-electron reduction of tellurium, which is consistent with the EDX result for the films deposited in this potential range. The side reaction with $M/z = 0$ implies that the reduction product is soluble in solution, such as Te^{2+} . We have carried out RRDE experiments, in which the potential of the disk is scanned from OCP (+0.9 V vs. SHE) to 0 V while the ring potential is set at +1.0 V. However, zero oxidation current was detected on the ring, implying that Te^{2+} was not produced. Thus, the peak R_1 is assigned to the reduction of Te, but with a current efficiency lower than 100%. The increasing M/z implies that the reduction to Te^0 becomes more dominant as the potential becomes more negative.

Fig. 7 shows the peak R_1 obtained at various scan rates, from 2 to 200 mV s^{-1} . The peak current is found to be linear with scan rate as shown in Fig. 8a. Fig. 8b shows the variation of peak position (E_p) vs. $\log(\text{scan rate})$, where a linear dependence is found at high scan rate while the peak position remains constant at low scan rates. Such a behavior is consistent with formation of a monolayer following the random adsorption model, irreversible case [25]. In Fig. 8c, as scan rate increases, the peak charge tends to a constant value of 2.1 mC cm^{-2} , close to the value for two close-packed (0001) monolayers of Te (0.94 mC cm^{-2}). At low scan rates, the formation of the monolayer may change the kinetics of the electrode leading to bulk deposition of Te, which explains the higher peak charge. Similar formation of monolayers have been found for Bi on GaAs substrates from aqueous solutions elsewhere in literature [26]. Dissolution of Te can be observed during the anodic scan with M/z values of -32 g mol^{-1} following the 4-electron oxidation of Eq. (4).

For the deposition of bismuth telluride films, the theoretical M/z value may vary from $+32$ to $+69.6 \text{ g mol}^{-1}$ depending on the alloy composition, from pure Te to pure Bi, respectively. For the stoichiometric composition Bi_2Te_3 , a value of $+44.6 \text{ g mol}^{-1}$ can be calculated from the reaction:

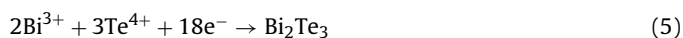


Fig. 9 shows the CV and M/z ratio obtained for a solution containing 50 mM $\text{Bi}(\text{NO}_3)_3$ and 50 mM TeCl_4 . At potentials more negative than +0.2 V, which is the reduction potential of Bi in the pure Bi solution, the M/z ratio increases from $+32$ to $+48 \text{ g mol}^{-1}$.

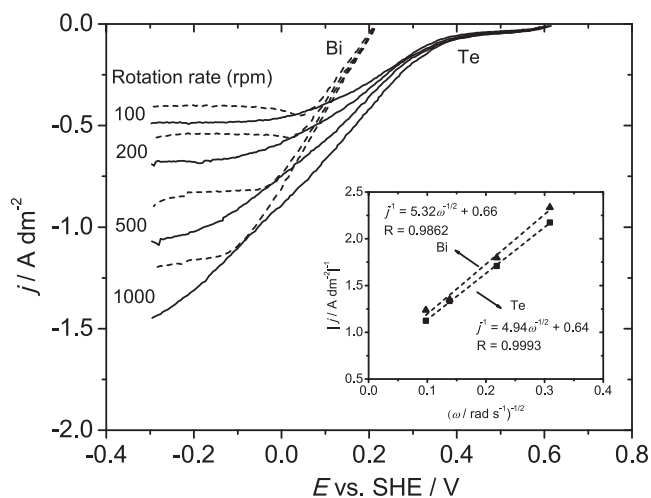


Fig. 10. Polarization curves obtained at different rotation speeds from 2 solutions containing either 0.05 M $\text{Bi}(\text{NO}_3)_3$ or 0.05 M TeCl_4 and 0.5 M LiNO_3 , at 50°C , scan rate 10 mV s^{-1} , Pt WE $\phi 4\text{ mm}$. The inset shows the plots and fits according to Eq. (6) for Bi and Te cases.

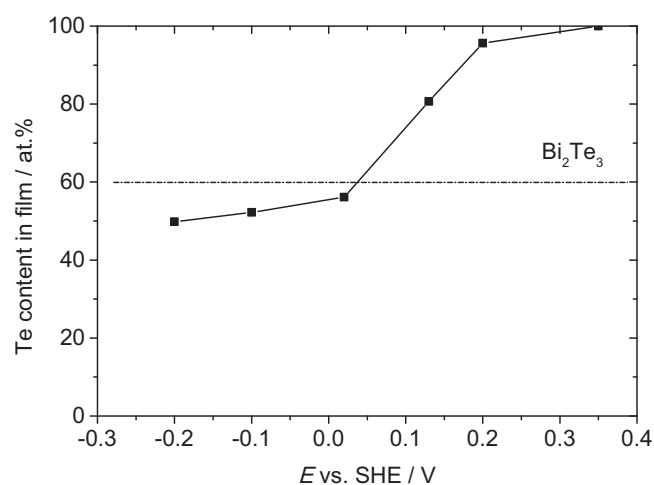


Fig. 11. Composition of Bi_xTe_y films deposited at different potentials from a mixed solution containing 0.05 M TeCl_4 , 0.05 M $\text{Bi}(\text{NO}_3)_3$, and 0.5 M LiNO_3 , at 50°C , non-stirred.

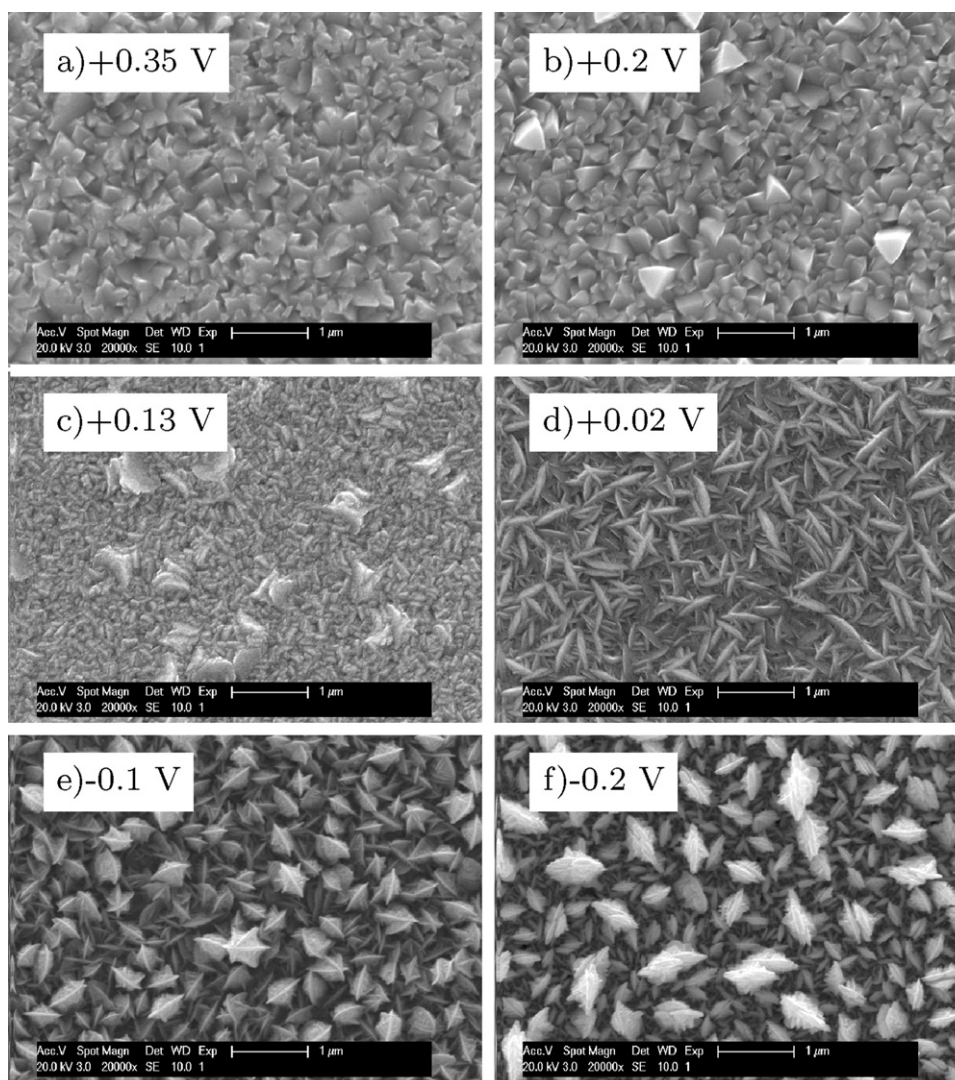


Fig. 12. SEM images of Bi_xTe_y films deposited from a mixed solution containing 0.05 M TeCl_4 , 0.05 M $\text{Bi}(\text{NO}_3)_3$, and 0.5 M LiNO_3 , at 50°C , non-stirred (scale bar $1\ \mu\text{m}$).

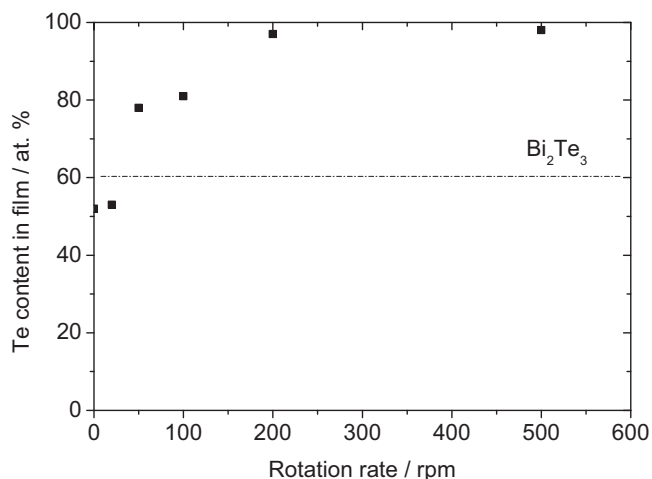


Fig. 13. Composition of Bi_xTe_y films deposited at 0.02 V vs. SHE, at different rotation rates from a mixed solution containing 0.05 M TeCl_4 , 0.05 M $\text{Bi}(\text{NO}_3)_3$, and 0.5 M LiNO_3 , at 50 °C, non-stirred (scale bar 1 μm).

This corresponds to deposition of Bi_xTe_y with increasing Bi content. At potentials more positive than +0.2 V, the CV and M/z ratio shows a very similar behavior to that obtained from the pure Te solution (Fig. 5). During the cathodic scan, M/z remains 0 as the potential is scanned from open circuit potential +0.9 V to +0.5 V, while the current increases slightly. Between +0.2 and +0.5 V, a mixed mechanism of two reduction processes is obtained with increasing M/z from 0 to +32 g mol^{-1} . It is likely that pure Te films are obtained in this potential range. In the anodic scan, the oxidation current increases constantly, starting from +0.6 V. The M/z ratio equals about -40 g mol^{-1} , corresponding to the dissolution of Bi_xTe_y alloys. Because the M/z value is smaller than 44.6 g mol^{-1} , it is predicted that the deposited film is probably Te-rich. This variation of the film composition was then confirmed by EDX analysis.

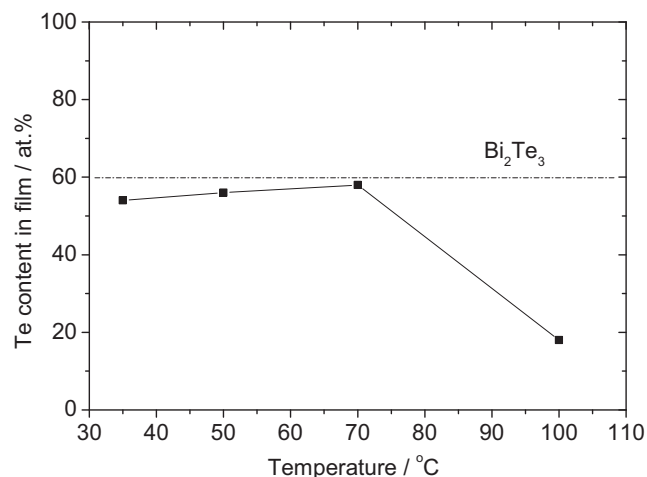


Fig. 14. Composition of Bi_xTe_y films deposited at different temperatures from a mixed solution containing 0.05 M TeCl_4 , 0.05 M $\text{Bi}(\text{NO}_3)_3$, and 0.5 M LiNO_3 , non-stirred.

To study the kinetics of the individual Bi and Te systems, polarization curves were measured with a rotating disk electrode at different rotation speeds. According to the Koutecky–Levich equation, the reciprocal of the current density j depends linearly on the reciprocal of the square root of the rotating speed ω [22]:

$$\frac{1}{j} = \frac{1}{0.62zFD^{2/3}\nu^{-1/6}C} \frac{1}{\omega^{1/2}} + \frac{1}{zFk} \quad (6)$$

where D is the diffusion coefficient ($\text{m}^2 \text{s}^{-1}$), ν is the kinematic viscosity ($\text{m}^2 \text{s}^{-1}$), C is the concentration (mol m^{-3}), ω is the rotation speed (rad s^{-1}), k is the rate constant (m s^{-1}). Eq. (6) predicts that plots of $1/j$ vs. $1/\omega^{1/2}$ will generate straight lines having slopes proportional to $1/D^{2/3}$ and intersects with y -axis proportional to $1/k$. Fig. 10 shows the polarization curves obtained

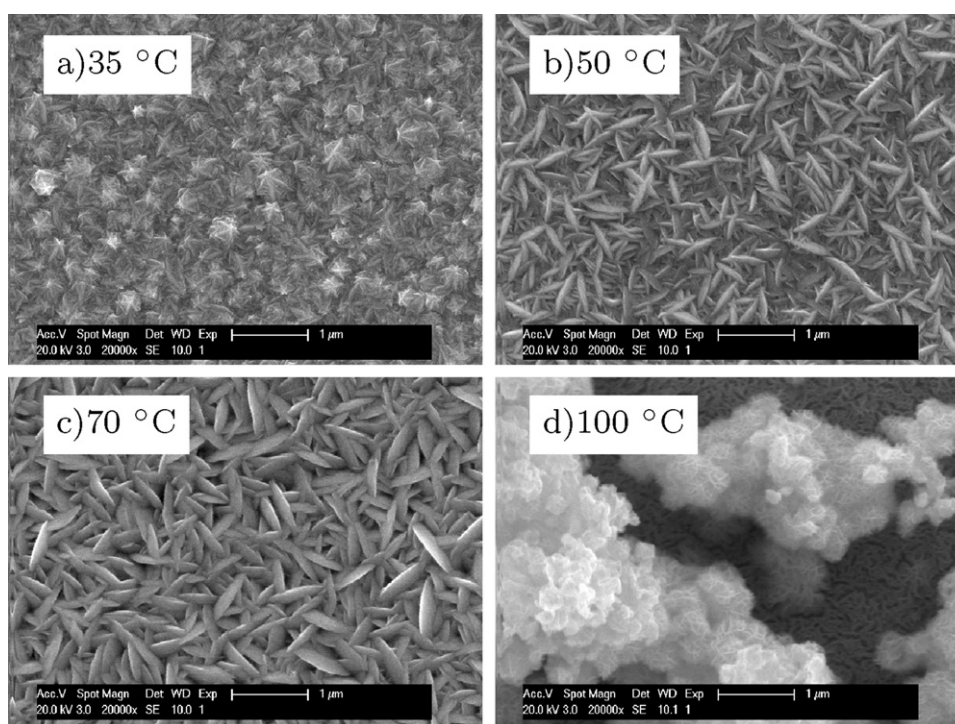


Fig. 15. SEM images of Bi_xTe_y films deposited at different temperatures from a mixed solution containing 0.05 M TeCl_4 , 0.05 M $\text{Bi}(\text{NO}_3)_3$, and 0.5 M LiNO_3 , non-stirred (scale bar 1 μm).

for Bi and Te solutions containing either 0.05 M $\text{Bi}(\text{NO}_3)_3$ or 0.05 M TeCl_4 and 0.5 M LiNO_3 at 50 °C on a Pt RDE (pre-coated with Bi or Te before each experiment). Dependence of $1/j$ vs. $1/\omega^{1/2}$ for both Bi and Te cases are plotted in the inset together with their linear fits following Eq. (6). For the case of bismuth, a diffusion coefficient $D_{\text{Bi}} = 1.3 \times 10^{-10} \text{ m}^2 \text{ s}^{-1}$ and a rate constant $k_{\text{Bi}} = 1.0 \times 10^{-5} \text{ m s}^{-1}$ were estimated. A diffusion coefficient $D_{\text{Te}} = 0.98 \times 10^{-10} \text{ m}^2 \text{ s}^{-1}$ and a rate constant $D_{\text{Te}} = 0.8 \times 10^{-5} \text{ m s}^{-1}$ were found for tellurium. These diffusion coefficients are comparable with $1.72 \times 10^{-10} \text{ m}^2 \text{ s}^{-1}$ [27] and $1.3 \times 10^{-10} \text{ m}^2 \text{ s}^{-1}$ [28] for bismuth and tellurium, respectively, in aqueous solutions.

3.2. Bismuth telluride electrodeposition

Bismuth telluride films were deposited under potentiostatic conditions from the mixed solution containing 50 mM $\text{Bi}(\text{NO}_3)_3$ and 50 mM TeCl_4 (0.5 M LiNO_3) at 50 °C. The same amount of charge was used for each deposition, so that the thickness of the deposits is comparable. Fig. 11 shows the variation of film composition with respect to applied potential. As predicted from the CV and M/z analysis (Section 3.1), Bi_xTe_y films can be deposited at potential more negative than +0.2 V. A strong influence of the potential on the film composition can be observed in the potential range between +0.2 and 0 V, where the Te content decreases from 98 at.% to about 58 at.%. At more negative potentials, the film composition is stable around 50 at.%, which can be explained by the nearly identical limiting mass transport for both ions as seen in Figs. 3 and 5.

Fig. 12 shows SEM images of the films deposited at different potentials. The Te-rich films deposited at +0.35 V and +0.2 V are very compact and have the typical morphology of Te films (compared e.g. to those in Fig. 6a and b). The film deposited at +0.13 V (80 at.% Te) shows a smooth background with hills (Fig. 12c). Point EDX analysis shows that the composition of the background is close to the stoichiometric ratio Bi_2Te_3 while the hills contained much more Te. A needle-like morphology is obtained for the $\text{Bi}_{2.1}\text{Te}_{2.9}$ film deposited at +0.02 V (Fig. 12d). This is a typical morphology for stoichiometric bismuth telluride films obtained from aqueous solutions [7,8]. At more negative potentials, the films become rougher with star-like texture.

Agitation is found to have very strong influence on the composition of the films deposited at constant potentials. Fig. 13 shows composition variation of the films deposited at +0.02 V vs. SHE using a rotating disk. Te content increases quickly with increasing rotation speed and nearly pure Te films are obtained once the substrate rotates faster than 200 rpm. This effect can be understood (at least in part) as a result of IR-drop effect in solution. In these experiments, when rotation speed increases from 0 to 500 rpm, the deposition current increases from 0.15 to 0.33 A dm^{-2} , leading to increase of IR drop from 0.13 to 0.34 V. Thus, actual deposition potentials are shifted to more positive range +0.15 to +0.36 V vs. SHE, which results in Te-rich or pure Te films as observed in Fig. 11 for the variation of film composition with respect to deposition potential.

The influence of temperature on the morphology and composition of Bi_2Te_3 films are presented in Figs. 14 and 15. The films were prepared potentiostatically at +0.02 V with the same amount of charge. EDX shows that the films deposited at temperatures below 70 °C have very similar composition, about 55 at.% Te while at 100 °C, the Te content drops to 18 at.%.

Bi_2Te_3 films deposited at 50 and 70 °C have the same needle-like morphology (Fig. 15). The needles in the film deposited at 50 °C have sharp edges while those in the films deposited at 70 °C are bigger. On the film deposited at 35 °C, small grains with very little needles can be observed. The film deposited at 100 °C shows a very rough surface.

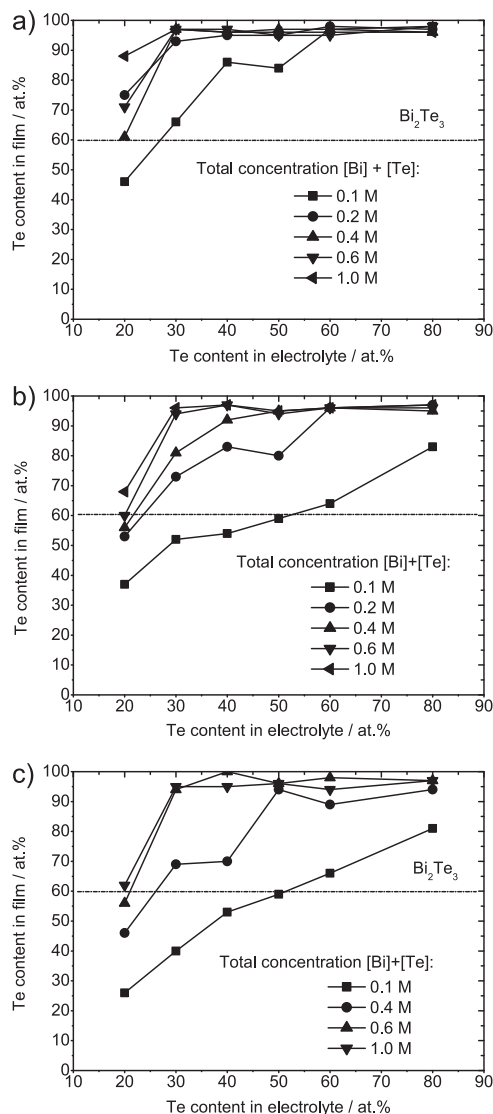


Fig. 16. Composition of Bi_xTe_y films with respect to bath composition and total concentration at different potentials $E = +0.13$ V (a), $E = +0.02$ V (b), and $E = -0.1$ V (c) vs. SHE, at 50 °C, non-stirred.

Fig. 16 shows the influence of the electrolyte composition (metal ion ratio and concentration) on the film composition at three different potentials. As expected, the Te content of the films increase with increasing Te concentration in solution. Such behavior is typical for regular alloy electrodeposition systems. The dependence of film composition on electrolyte composition is more obvious at lower total concentration. In more concentrated solutions (0.6 and 1 M of $\text{Bi}(\text{NO}_3)_3$ and TeCl_4), Te-richer films are obtained. Because the films were deposited at constant potential, the problem of IR drop might play a role here as deposition current, so IR drop, was increasing with increasing total metal concentration. The actual deposition potential, thus, shifted to more positive potentials, resulting in Te-richer films. When the applied potentials become more negative (Fig. 16a–c), the Te content in the film decreases. This shows that stoichiometric bismuth telluride films can be obtained by optimizing electrolyte composition, total concentration and applied potential.

High rate electrodeposition of bismuth telluride films was performed under galvanostatic conditions at a current density of 5 A dm^{-2} from a solution containing 0.4 M $\text{Bi}(\text{NO}_3)_3$ and 0.2 M TeCl_4 , with 0.5 M LiNO_3 as conducting salt. This current density is

equivalent to a growth rate of $108.5 \mu\text{m h}^{-1}$, which is more than twice the highest deposition rate reported in literature ($50 \mu\text{m h}^{-1}$ by Glatz et al. via pulsed electrodeposition from a 2 M HNO_3 solution [9]). EDX analysis shows that the Te content in the films is 67 at.%, which is very close to the best n-type bismuth telluride materials.

Stability of the EG electrolytes was investigated by long term electrodeposition. Thick Bi–Te films were prepared in potentiostatic mode. Thickness measured along the 15 mm length of the film shows uniform values of about $67 \mu\text{m}$. No cracks were observed, implying low internal stress in the film. The composition of the film was found to be uniform across the thickness and equal to 75 at.% Te.

The semiconductor type of the deposited films were confirmed by Seebeck coefficient measurement described in [29]. Positive values, i.e. p-type behavior, are observed for the films deposited at constant potential (-0.3 V to -0.9 V vs. SHE) from a solution containing 0.05 M $\text{Bi}(\text{NO}_3)_3$, 0.05 M TeCl_4 , 0.5 M LiNO_3 , at 50°C on a rotating disk electrode at 200 rpm. The highest value that was obtained in the as-deposited state is $+240 \mu\text{V/K}$, which is comparable to what is reported in literature for this material. Films deposited at potentials more negative than -1.0 V vs. SHE show n-type behavior with negative Seebeck coefficients.

4. Conclusions

We examined a non-aqueous electrolyte using ethylene glycol for the electrodeposition of thermoelectric bismuth telluride films. Both bismuth and tellurium are reduced in one-step from Bi^{3+} and Te^{4+} at potentials more negative than $+0.2 \text{ V}$ and $+0.55 \text{ V}$ vs. SHE, respectively. Te reduction is preceded by the formation of a monolayer of about 2 atomic layers, which follows a random irreversible adsorption model. Within the potential range $+0.3$ to $+0.55 \text{ V}$ vs. SHE, there is evidence of a side-reaction that happens together with the reduction of Te and leads to a current efficiency of less than 100%. The kinetics of the electrodeposition reactions were studied from rotating disk electrode experiments by applying the Koutecky–Levich equation. The diffusion coefficient and reduction rate constant of Bi and Te are similar and are close to those found in aqueous solutions.

Stoichiometric Bi_2Te_3 films are obtained from various concentrated EG electrolytes containing up to 1 M total concentration of bismuth and tellurium ions. Film composition can be controlled by either applied potential (current) or electrolyte composition as the Te content of the film increases as the potential becomes more cathodic or with increasing Te/Bi ratio in solution. Thick Bi_xTe_y films can be prepared with low internal stress and uniform composition profile across the cross-section. Both p- and n-type thermoelectric materials are obtained, as confirmed by Seebeck coefficient measurement.

Acknowledgments

This research was funded by a Ph.D. grant of the imec/Holst center to HPN. The authors acknowledge financial support by the KU Leuven (Projects IDO/05/005 and GOA 08/05), by the FWO-Flanders (research community “Ionic Liquids”), by the IWT-Flanders (SBO-project IWT 80031 “MAPIL”) and the support of the Belgian Federal Science Policy Office through the IUAP project INANOMAT (contract P6/17).

References

- [1] D.M. Rowe (Ed.), *CRC Handbook of Thermoelectrics*, CRC Press, Boca Raton, 1995.
- [2] F. Xiao, C. Hangarter, B. Yoo, Y. Rheem, K.-H. Lee, N.V. Myung, *Electrochim. Acta* 53 (2008) 8103.
- [3] C. Boulanger, *J. Electron. Mater.* 39 (2010) 1818.
- [4] M. Gonzalez, A. Prieto, R. Gronsky, T. Sands, A.M. Stacy, *J. Electrochem. Soc.* 149 (2002) 546.
- [5] K. Tittes, A. Bund, W. Plieth, A. Bienten, S. Paschen, M. Plotner, H. Grafe, W.J. Fischer, *J. Solid State Electrochem.* 7 (2003) 714.
- [6] S. Michel, S. Diliberto, C. Boulanger, N. Stein, J.M. Lecuire, *J. Cryst. Growth* 277 (2005) 274.
- [7] B.Y. Yoo, C.K. Huang, J. Lim, J. Herman, M. Ryan, J.P. Fleurial, N. Myung, *Electrochim. Acta* 50 (2005) 4371.
- [8] W.L. Wang, C.C. Wan, Y.Y. Wang, *Electrochim. Acta* 52 (2007) 6502.
- [9] W. Glatz, L. Durrer, E. Schwyter, C. Hierold, *Electrochim. Acta* 54 (2008) 755.
- [10] R. Chen, D. Xu, G. Guo, L. Gui, *Electrochim. Acta* 49 (2004) 2243.
- [11] P. Grez, R. Henriquez, E.A. Dalchiele, H. Gomez, *J. Chil. Chem. Soc.* 52 (2007) 1246.
- [12] O.I. Kuntiyi, E.V. Okhremchuk, V.T. Yavorskii, *Russ. J. Appl. Chem.* 80 (2007) 1327.
- [13] M.M. Gonzalez, A.L. Prieto, M.S. Knox, R. Gronsky, T. Sands, A.M. Stacy, *Chem. Mater.* 15 (2003) 1676.
- [14] W.-J. Li, *Electrochim. Acta* 54 (2009) 7167.
- [15] F.-H. Li, W. Wang, *Electrochim. Acta* 55 (2010) 5000.
- [16] H.P. Nguyen, Z. Wang, J. Su, R.J.M. Vullers, P.M. Vereecken, J. Fransaer, *ECS Trans.* 33 (2010).
- [17] S. Pawar, A. Moholkar, P. Shinde, K. Rajpure, C. Bhosale, *J. Alloys Compd.* 459 (2008) 515.
- [18] H. Yamamoto, R. Iguchi, M. Morishita, *ECS Trans.* 16 (2009) 191.
- [19] T.N. Vorobyova, O.N. Vrublevskaia, *Surf. Coat. Technol.* 204 (2010) 1314.
- [20] K. Premaratne, S.N.A.I.M. Dharmadasa, A.P. Samantilleka, *Renew. Energy* 29 (2003) 549.
- [21] G. Vatankehah, J. Lessard, G. Jerkiewicz, A. Zolfaghari, B.E. Conway, *Electrochim. Acta* 48 (2003) 1613.
- [22] S. Treimer, A. Tang, D.C. Johnson, *Electroanalysis* 14 (2002) 165.
- [23] J. Agrisuelas, C. Gabrielli, J.J. Garcia-Jareño, D. Giménez-Romero, J. Gregori, H. Perrot, F. Vicente, *J. Electrochem. Soc.* 154 (2007) F134.
- [24] M. Pourbaix, *Atlas of Electrochemical Equilibria in Aqueous Solutions*, National Association of Corrosion Engineers, Houston, 1974.
- [25] M. Noel, K.I. Vasu, *Cyclic Voltammetry and the Frontiers of Electrochemistry*, Aspect Publications, London, 1990.
- [26] P.M. Vereecken, S. Ren, L. Sun, P.C. Searson, *J. Electrochem. Soc.* 150 (2003) C131.
- [27] E. Sandnes, M.E. Williams, U. Bertocci, M.D. Vaudin, G.R. Stafford, *Electrochim. Acta* 52 (2007) 6221.
- [28] S. Wen, R.R. Corderman, F. Seker, A.P. Zhang, L. Denault, M.L. Blohm, *J. Electrochem. Soc.* 153 (2006) 595.
- [29] H.P. Nguyen, J. Su, Z. Wang, R.J. Vullers, P.M. Vereecken, J. Fransaer, *J. Mater. Res.* 26 (2011) 1953.